IEEE Access
Multidisciplinary ⋮ Rapid Review ⋮ Open Access Journal

Received 7 September 2022, accepted 6 October 2022, date of publication 19 October 2022, date of current version 26 October 2022.

Digital Object Identifier 10.1109/ACCESS.2022.3215511

RESEARCH ARTICLE

Using a Bivariate Polynomial in an EKF for State and Inductance Estimations in the Presence of Saturation Effects to Adaptively Control a PMSM

TANJA ZWERGER[1] AND PAOLO MERCORELLI[2], (Member, IEEE)
[1]Department of Development, Rolls Royce Solutions GmbH, 88045 Friedrichshafen, Germany
[2]Institute of Product and Process Innovation, Leuphana University of Lueneburg, 21335 Lueneburg, Germany
Corresponding author: Paolo Mercorelli (mercorelli@uni.leuphana.de)

ABSTRACT This paper takes into consideration a combined extended Kalman filter (CEKF) by using a bivariate polynomial for the estimation of L_d and L_q in saturation conditions. In the context of the Kalman filter (KF), L_d and L_q are modelled as nonlinear augmented states to control a permanent magnetic synchronous machine (PMSM). Once L_d and L_q are estimated, continuous monitoring of the machine saturation conditions is achieved to ensure the desired torque even under saturation conditions. The proposed adaptive control method based on maximum torque per ampere (MTPA) consists of an adaptive feedforward and PI controller. A discussion in light of the measured results using Hardware-in-the-loop is also included.

INDEX TERMS PMSM, extended Kalman filter, parameter estimation, bivariate polynomial.

I. INTRODUCTION

Permanent magnetic synchronous machines (PMSMs) have become increasingly important for applications with limited space and high energy density requirements [1]. PMSMs are therefore a welcome solution in the selection of a suitable electric drive, and not only in the automotive sector, where the increase in the influence of electromobility is becoming more and more apparent [2]. PMSMs with reluctance torque are used in areas where high energy density and, above all, high electrical torque is required over the widest possible speed range.

A. PMSM CONTROL STRATEGIES

Taking into account the control part of the PMSM, it is necessary to reduce the copper losses in the stator of the machine, since they are the dominant loss component and increase quadratically with the machine current. This leads to a control strategy with a minimum stator current in order to obtain a defined electrical torque, which is also referred to as maximum torque per ampere (MTPA) control [3]. The MTPA trajectory was calculated in a normalized form and given as a lookup table into the calculation for the desired currents i_{dd} and i_{qd}, as it can be seen in Fig. 1. A different approach is maximum torque per voltage (MTPV). This technique is proposed for the control of the drive in a high speed range, based on direct-flux field-oriented vector control as in [4] or in [5].

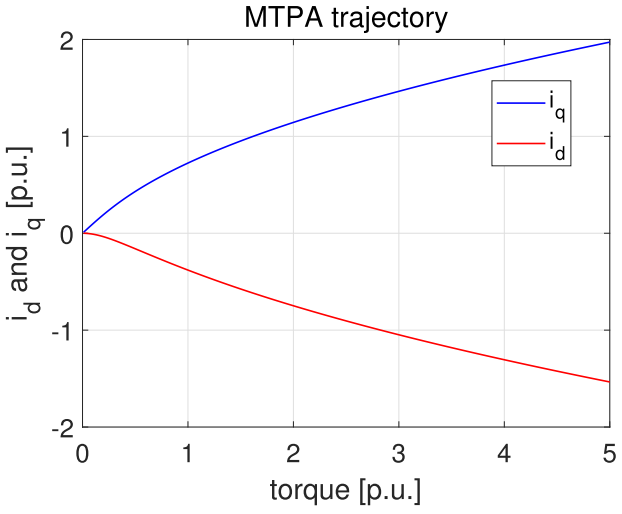

FIGURE 1. MTPA trajectory.

The associate editor coordinating the review of this manuscript and approving it for publication was Zhiguang Feng.

Recently, concerning control, in [6] and in [7] a combination of sliding mode control (SMC) and MTPA strategies are proposed and in [8] an adaptive feedforward control strategy is proposed. In [9] a control scheme for PMSMs using model predictive control (MPC) and a feedforward action in the presence of saturated inputs is presented. Knowledge of the course of the time-varying parameters plays an important role in the operation with MTPA and MTPV as well as in the feedforward control. There are different approaches to obtain the saturated course of the inductance of an electrical machine for the control. A highly-granular measurement of the inductance is a sufficient but very time-consuming method. In conventional control, a measurement is performed for the L_d and L_q values to adapt and optimize the control. For complex machines with a high reluctance component, a more accurate determination of these parameters is required, which can entail a time-consuming measurement of several weeks and would have to be carried out again if structural changes are made to the PMSM. For instance, in [10], inductances are modelled as functions of q-axis current based on the flux data obtained experimentally and using a lookup table based method. The calculation of flux linkage is proposed and thus the corresponding inductances are identified. In [11] a field-weakening scheme based on a 3-D lookup table is used to control a PMSM. In [12] conventional torque control methods based on 2D-lookup table are proposed considering DC-Link voltage variation.

B. INDUCTANCE ESTIMATION

In [13] the parameter observability in an α-β-frame is proven before an estimation process with a recursive least squares (RLS) method is presented. Very recently in [14] an estimation of inductance is used to obtain the estimated position. The estimated methods do not consider the presence of noise. Other estimation possibilities, as well as a comparative study, are given in [15], however, there are no considerations of the saturation effects of the inductance. A possibility with an RLS method for the consideration of the current dependent values by regarding the dependence of the inductance in only d- or q- direction is shown in [16]. The statement is made that the current dependence for L_d in q- current direction as well as the current dependence for L_q in d- current direction can be neglected for many PMSM models. This may be a valid possibility for a particular type of machine where the saturation effects occur only in one current direction. An advanced method is represented by an extended Kalman Filter (EKF), which is a popular algorithm often used to estimate parameters and state variables even in the presence of unknown inputs, see [17]. The EKF is a set of mathematical equations that provides an efficient computational recursive algorithm, which generates a solution of the least-squares method. The algorithm is a powerful one, which supports estimations of time-dependent states and it can do so when the nature of the modeled system is not precisely known [18]. In the following, a method is described which, by calculating a bivariate polynomial and using an EKF, allows the

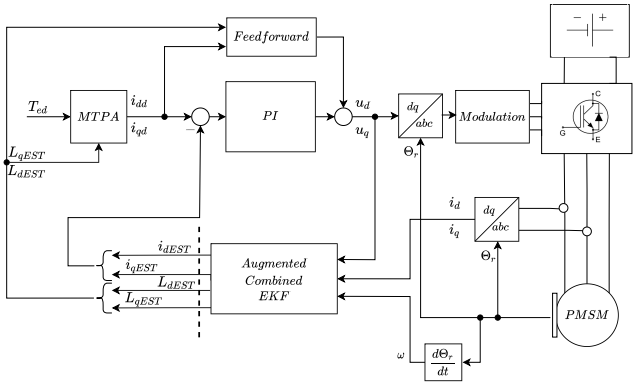

FIGURE 2. Control setup.

determination of the saturated inductance of a PMSM, which depends on the d- as well as on the q- current. A forward Euler discretisation is presented. The calculated polynomial is deliberately calculated from fewer interpolation points in order to significantly reduce the measurement effort. The resulting uncertainty between the grid points is compensated by the EKF used. In Fig. 2, the experimental setup for the proof of function of the EKF estimation is presented. In the outer control loop an MTPA control defines the desired saturated current input for the current control, which is calculated from the desired input torque. It should be noticed that the estimated currents are also used to calculate L_d and L_q through the characteristics of the motor. As it is possible to see from Fig. 2, the proposed adaptive control scheme, based on MTPA with saturating optimal currents i_d and i_q as reference currents, consists of an adaptive MTPA, feedforward and PI controller to work in saturation conditions when these occur. Concerning the analysis of the observability, [19], [20] and [21] showed that the PMSM system in stator-fixed α, β-coordinates is observable with respect to the states i_α, i_β, ω, θ using only measurements of the currents $i_{\alpha,\beta}$, as long as the velocity ω is not zero or $L_d \neq L_q$. The qualitiy of the state estimation depends on the modelled system. In the context of electrical machines, a Kalman filter (KF) is used to estimate unmeasurable states for control and also to estimate parameters such as resistance and inductance, which are needed in a model-based control strategy to adapt the control law in accordance with possible parameter changes which can occur. The modern control techniques for electrical motors are model based ones and often combined with sensorless control strategies to reduce the number of sensors, [22], [23] and more recently in [24] and [25] and also in [26].

C. MAIN CONTRIBUTION AND STRUCTURE OF THE PAPER

The main contribution of this paper can be summarised in the following points:

- to continuously monitor saturation conditions of the machine through the estimation of inductances L_d and L_q using an EKF because of the presence of measured noise and to deal process uncertainties

- to propose a control scheme based on MTPA with saturating optimal currents i_d and i_q as reference currents for an adaptive feedforward and PI controller.

Basically our main contribution consists of the use of the bivariate polynomial in the context of the Kalman filter to estimate the parameters of the machine in order to realize an adaptive feedforward control combined with a PI controller. The results are validated by prototyping the control with a TI DSP F28335. The paper is organised in the following way: Section II is devoted to the description of the machine with its mathematical model; in Section III the two bivariate polynomials are derived for the modelling of L_d and L_q; measured results close the paper together with the conclusions. An appendix is included at the end to report a part of the calculation to implement the Jacobian matrices of the EKF.

The main nomenclature

$u_d(t)$	Direct voltage input.
$u_q(t)$	Quadrature voltage input.
$i_d(t)$	Direct current.
$i_q(t)$	Quadrature current.
$i_{dd}(t)$	Desired direct current.
$i_{qd}(t)$	Desired quadrature current.
$\omega_r(t)$	Mechanical angular velocity of the rotor.
$\omega_{el}(t)$	Electrical angular velocity of the rotor.
p	Couple of magnetic poles ($\omega_{el}(t) = p\omega_r(t)$).
R_s	Stator resistance.
$L_d(t)$	Direct axis self-inductance.
$L_q(t)$	Quadrature axis self-inductance.
ψ_p	Main flux constant.
$T_e(t)$	Electric torque.
θ_d	Coefficient polynomial for calculation of $L_d(t)$.
θ_q	Coefficient polynomial for calculation of $L_q(t)$.
θ_r	Mechanical angle of the rotor.

II. DESCRIPTION OF THE MODEL OF THE PMSM

The most commonly used model in field-oriented control is the dq model, which is developed from the three-phase e-machine model with the help of the Clarke-Park transformation. The equations which are obtained for the currents i_d and i_q are written in (1) and (2) for a constant parameter of L_d and L_q.

$$\frac{di_d(t)}{dt} = \frac{u_d(t)}{L_d(t)} - \frac{i_d(t)R_s}{L_d(t)} + \frac{\omega_{el}(t)L_q(t)i_q(t)}{L_d(t)}. \tag{1}$$

$$\frac{di_q(t)}{dt} = \frac{u_q(t)}{L_q(t)} - \frac{i_q(t)R_s}{L_q(t)} - \frac{\omega_{el}(t)L_d(t)i_d(t)}{L_q(t)} - \frac{\omega_{el}(t)\psi_p}{L_q(t)}. \tag{2}$$

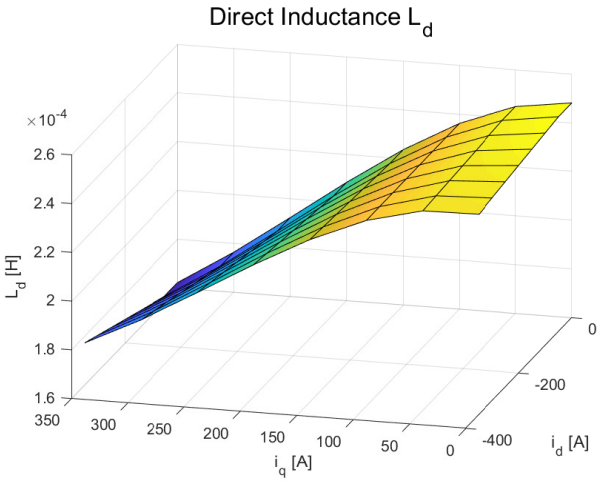

FIGURE 3. Course of the characteristic field for L_d.

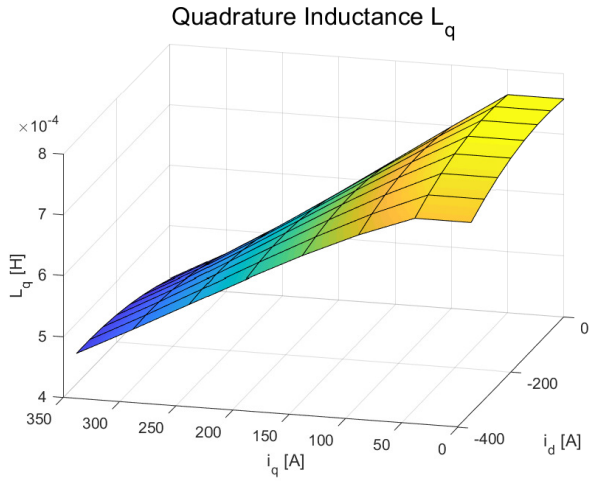

FIGURE 4. Course of the characteristic field for L_q.

At high flux densities, as occur when high torque is required, saturation effects occur in the iron of the electric machine, which means that the inductance must be considered as a function of the currents i_d and i_q:

$$L_{d,q} = f(i_d, i_q). \tag{3}$$

The course of the inductance in dependence of the currents is presented in Fig. 3 and Fig. 4. The components $\frac{dL_d}{dt}$ and $\frac{dL_q}{dt}$ are neglected in order to simplify the model to be used in the EKF. It is to note that the EKF is able to manage such kind of simplifications to include them in its process noise. A good explanation for the consideration of the magnetic conditions is given in [27]. The electromagnetic torque is calculated in (4) and consists of the main torque as well as the reluctance torque due to the different inductances L_d and L_q.

$$T_e(t) = \frac{3}{2}p\Big\{i_q(t)\psi_p + (L_d(t) - L_q(t))i_d(t)i_q(t)\Big\}. \tag{4}$$

III. CALCULATION OF THE BIVARIATE POLYNOMIAL

The general form of a bivariate polynomial is given by:

$$f := n \to \sum_{j=0}^{n} \left(\sum_{i=0}^{m} a_{i,j} x^i y^j \right) \tag{5}$$

and the first and the second order bivariate polynomial with $n := 1$ and $m := 1$

$$f(1) = a_{1,1}xy + a_{1,0}x + a_{0,1}y + a_{0,0}. \tag{6}$$

And with $n := 2$ and $m := 2$

$$\begin{aligned} f(2) = {} & a_{2,2}x^2y^2 + a_{2,1}x^2y + a_{1,2}xy^2 \\ & + a_{2,0}x^2 + a_{1,1}xy + a_{0,2}y^2 + a_{1,0}x + a_{0,1}y + a_{0,0}. \end{aligned} \tag{7}$$

coefficients $a_{2,2}, a_{2,1}, a_{1,2}, a_{2,0} \ldots, a_{0,0} \in \mathbb{R}$. For $a_{n,m} \neq 0$, $n \in \mathbb{N}$, $m \in \mathbb{N}$, define the bivariate grade of the polynomial. A possible formal definition and more details can be found in [28].

To calculate the bivariate polynomial for the current dependent inductance, the coefficients in (8) with Θ_d and Θ_q have to be calculated.

$$\begin{bmatrix} \Theta_d \\ \Theta_q \end{bmatrix} = \begin{bmatrix} X_{d/q}^T X_{d/q} \\ X_{d/q}^T X_{d/q} \end{bmatrix}^{-1} \begin{bmatrix} X_{d/q}^T L_{dD} \\ X_{d/q}^T L_{qD} \end{bmatrix}. \tag{8}$$

$X_{d/q}$ is calculated with the current vectors I_d and I_q:

$$I_d = \begin{bmatrix} -350 & -150 & 0 \end{bmatrix} \tag{9}$$

and

$$I_q = \begin{bmatrix} 0 & 200 & 350 \end{bmatrix}. \tag{10}$$

The direct and quadrature current vectors include 8 elements, so the matrix for $X_{d/q}$ is calculated as follows:

$$X_{d/q} = \begin{bmatrix} I_q(1)I_d^T & I_d^T & I_q(1)I_{3\times1} & I_{3\times1} \\ I_q(2)I_d^T & I_d^T & I_q(2)I_{3\times1} & I_{3\times1} \\ I_q(3)I_d^T & I_d^T & I_q(3)I_{3\times1} & I_{3\times1} \end{bmatrix}. \tag{11}$$

with $I_d(1)$, $I_d(2)$, $I_d(3)$ and $I_q(1)$, $I_q(2)$, $I_q(3)$ as the single element of the current vectors I_d and I_q and $I_{3\times1}$ as a column with 3 elements, each being one. L_{dD} as well as L_{qD} are vectors with 9 elements, in which the dependence of the inductance of the currents is reproduced. For the calculation of the bivariate polynomial of the inductances L_d and L_q the defined example in (6) has to be adapted the following way, where the first number on the inductance indicates the dependence in direction of current i_d and the second number indicates the dependence in direction of the current i_q as (12), shown at the bottom of the page.

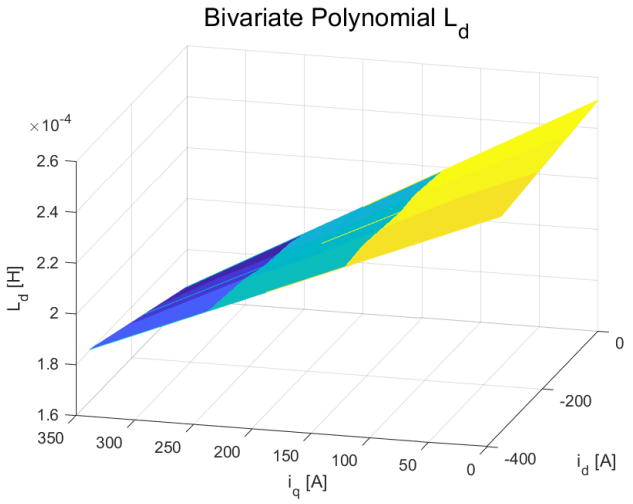

FIGURE 5. Calculated bivariate polynomial L_d.

In dependence of the current i_d the following structure is obtained as (13), shown at the bottom of the page, with $\Theta_d(1)$, $\Theta_d(2)$, …, $\Theta_d(4)$ and $\Theta_q(1)$, $\Theta_q(2)$, …, $\Theta_q(4)$ as the single elements of the calculated vectors Θ_d and Θ_q.

The inductances L_d and L_q are calculated in dependence for its current vectors I_d and I_q. The current is no longer time dependent, since L_d and L_q are calculated offline in a static least squares procedure. The inductance L_q then can be written as

$$L_q(t) = \Theta_q(1)i_d(t)i_q(t) + \Theta_q(2)i_q(t) + \Theta_q(3)i_d(t) + \Theta_q(4). \tag{14}$$

For the inductance L_d the bivariate polynomial can be calculated in a similar way. In a short form, it can be written

$$L_d(t) = \Theta_d(1)i_d(t)i_q(t) + \Theta_d(2)i_d(t) + \Theta_d(3)i_q(t) + \Theta_d(4). \tag{15}$$

The calculated bivariate polynomials for the inductances L_d and L_q are given in Fig. 5 and in Fig. 6.

$$\begin{bmatrix} L_q(1,1) \\ L_q(1,2) \\ L_q(1,3) \end{bmatrix} = \begin{bmatrix} \Theta_q(1)I_d(1)I_q(1) + \Theta_q(2)I_d(1) + \Theta_q(3)I_q(1) + \Theta_q(4) \\ \Theta_q(1)I_d(1)I_q(2) + \Theta_q(2)I_d(1) + \Theta_q(3)I_q(2) + \Theta_q(4) \\ \Theta_q(1)I_d(1)I_q(3) + \Theta_q(2)I_d(1) + \Theta_q(3)I_q(3) + \Theta_q(4) \end{bmatrix}. \tag{12}$$

$$\begin{bmatrix} L_d(1,1) \\ L_d(2,1) \\ L_d(3,1) \end{bmatrix} = \begin{bmatrix} \Theta_d(1)I_d(1)I_q(1) + \Theta_d(2)I_d(1) + \Theta_d(3)I_q(1) + \Theta_d(4) \\ \Theta_d(1)I_d(2)I_q(1) + \Theta_d(2)I_d(2) + \Theta_d(3)I_q(2) + \Theta_d(4) \\ \Theta_d(1)I_d(3)I_q(1) + \Theta_d(2)I_d(3) + \Theta_d(3)I_q(3) + \Theta_d(4) \end{bmatrix}. \tag{13}$$

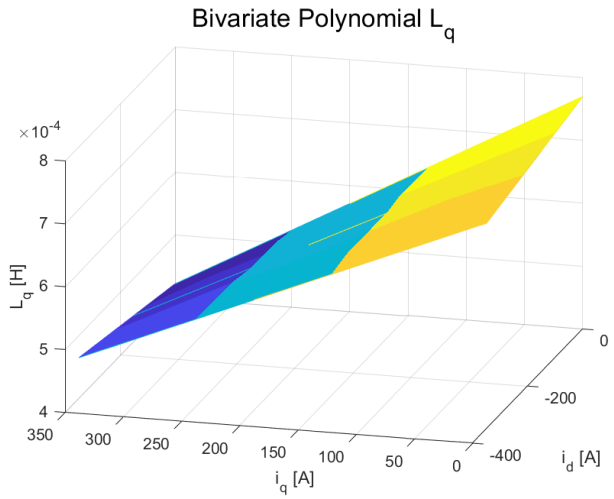

FIGURE 6. Calculated bivariate polynomial L_q.

IV. CEKF WITH FORWARD EULER DISCRETISATION

The forward Euler discretisation is an explicit calculation which is more commonly used if compared with other discretisation methods. Before calculating the implemented structure of the proposed EKF, a basic background of it is summarised here below. A tutorial on possible variations of different KFs can be found in [29].

A. EKF BACKGROUND

As we can see in [18], the a priori estimation of the state is as follows:

$$\hat{x}^-(k+1) = f(\hat{x}^-(k), u(k), w(k)), \quad k \in \mathbb{N} \tag{16}$$

in which function $f(\hat{x}^-, u, w)$ represents a nonlinear field used to model the considered system. Once Jacobian matrix J is calculated, the a priori error covariance of the state prediction is as follows:

$$P^-(k+1) = J(k+1)P(k)J(k+1)^T + Q, \tag{17}$$

where P represents the a posteriori error covariance matrix at step k (previous step). Matrix Q is specified by the covariance matrix of the measurement noise and can be considered as a quantification of the model uncertainty. The smaller the values of the trace in the matrix, the higher the reliability of the model. Lastly, the Kalman gain K, which minimises the a posteriori error covariance is calculated as:

$$K(k+1) = P^-(k+1)H^T(HP^-(k+1)H^T + R_w)^{-1}, \tag{18}$$

with R_w as the variance and covariance matrix for the measurement noise. Matrices R_w and Q define the tuning parameters. The matrix H defines the output Jacobian and indicates which state serves as the measurement in the EKF algorithm. The a posteriori estimation is as follows:

$$\hat{x}(k+1) = \hat{x}^-(k+1) + K(k+1)(z(k+1) - H\hat{x}^-(k+1)), \tag{19}$$

where

$$z_k(k+1) = x(k+1) + v(k+1) \tag{20}$$

represents the measured data in which vector signal v represents the measured *white Gaussian noise* associated with the sensoring system and which is assumed to be independent of *process noise* as defined above. Finally, the a posteriori estimation of the error covariance is as follows:

$$P(k+1) = (I - K(k+1)H)P^-(k+1). \tag{21}$$

The combined extended Kalman filter (CEKF) divides the estimated states in a model for the estimation of the mechanical states like *load*, θ_r and ω_r and another model for the estimation of the electrical states like the currents i_d, i_q as well as the inductances L_d and L_q. A CEKF, even though in another context, is also described in [6].

B. THE PROPOSED CEKF

The following equations describe the electrical model which is described with a forward Euler discretisation and the sample time T_s. For discretisation with forward Euler we get the following equations for the currents in (22) and (23):

$$\tilde{i_d}(k) = \frac{i_d(k+1) - i_d(k)}{Ts} = \frac{u_d(k)}{L_d(k)} - \frac{i_d(k)R_s}{L_d(k)} + \frac{\omega_{el}(k)L_q(k)i_q(k)}{L_d(k)}. \tag{22}$$

$$\tilde{i_q}(k) = \frac{i_q(k+1) - i_q(k)}{Ts} = \frac{u_q(k)}{L_q(k)} - \frac{i_q(k)R_s}{L_q(k)} - \frac{\omega_{el}(k)L_d(k)i_d(k)}{L_q(k)} - \frac{\omega_{el}(k)\psi_p}{L_q(k)}. \tag{23}$$

For the calculated inductances L_d and L_q in (15) and (14) in forward Euler discretisation by considering its derivation we get (24)–(26), as shown at the bottom of the next page, with $\tilde{i_d}$ and $\tilde{i_q}$ as derivations (22) and (23) for the currents i_d and i_q. The discrete nonlinear system equations in (26) are taken for the estimation of the a-priori states $\hat{x}^-(k+1)$ in the extended Kalman filter in the prediction step. The initial values $\hat{x}^+(0)$ are given by the nominal values for L_d and L_q in the data sheet and a value unequal 0 for the currents i_d and i_q. For the estimation of the a-priori states $\hat{x}^-(k+1)$ in the prediction step, the EKF uses the a-posteriori estimation $\hat{x}^+(k)$ of the last iteration. The electrical model is described by nonlinear system equations, that make it necessary for the estimation process of the EKF to derive the Jacobian matrix as (27), shown at the bottom of the next page. After calculating the Jacobian matrix by using the estimation results of the last iteration, we get the following 4×4 matrix for the electrical system as (28), shown at the bottom of the next page.

For sake of brevity, the elements $J_{f_{13}}$ and $J_{f_{24}}$ to $J_{f_{44}}$ are not reported in detail.

V. MEASUREMENT AND RESULTS

A. HARDWARE-IN-THE-LOOP REAL-TIME VALIDATION

As already explained in the introductional part, our main contribution consists of the use of the bivariate polynomial in the context of the Kalman filter to estimate the parameters of the machine in order to realize an adaptive feedforward control combined with a PI controller. The results are validated by prototyping the control with a TI DSP F28335. Figure 2 shows the main control setup for the taken measurements. The estimated values for the inductance are added into the MTPA, which works in an outer control loop and the feedforward control of the inner control loop. They shall guarantee the decoupling of the cross coupled d and q branches of the PMSM.

In order to be able to make a valid statement about the course and accuracy of the estimated inductance in comparison with the actual saturated parameters, a Hardware-in-the-loop (HIL) environment with Typhoon HIL 402 [30] as shown in Fig. 7 was chosen. HIL is a model-based, automated closed-loop test solution. The HIL simulation is often referred to as a plant system. It mimics the system to which the controller will be connected after testing is complete. This configuration allows HIL testing to determine how the actual controller will behave with the future system, with much greater accuracy than would be possible in a fully simulated laboratory environment [31]. The HIL 402 runs with the Software Version V2020.3. Within the HIL 402 hardware taken from Typhoon, a nonlinear kind of machine emulation is chosen. This choice is done considering the machine which is in use in Rolls Royce in order to advance and to implement control strategies. The control runs on a DSP and was compiled from Simulink into C code using an embedded coder. It operates on a DSP from Texas Instruments. The DSP has the designation F28335.

The specific parameters of the PMSM are given in Table 1.

TABLE 1. PMSM parameters.

flux distribution	sinusoidal	
stator resistance R_s	0.016	$[\Omega]$
inductance L_d	0.223e-3	$[H]$
inductance L_q	0.751e-3	$[H]$
flux induced by magnets Ψ_p	0.058	$[\frac{Vps}{rad}]$
inertia J	0.071	$[kgm^2]$
number of pole pairs p	4	

$$\frac{L_d(k+1)-L_d(k)}{Ts} = \Theta_d(1)i_q(k)\tilde{i_d}(k) + \Theta_d(1)i_d(k)\tilde{i_q}(k) + \Theta_d(2)\tilde{i_d}(k) + \Theta_d(3)\tilde{i_q}(k). \tag{24}$$

$$\frac{L_q(k+1)-L_q(k)}{Ts} = \Theta_d(1)i_q(k)\tilde{i_d}(k) + \Theta_d(1)i_d(k)\tilde{i_q}(k) + \Theta_d(2)\tilde{i_d}(k) + \Theta_d(3)\tilde{i_q}(k). \tag{25}$$

$$\begin{bmatrix} i_d(k+1) \\ i_q(k+1) \\ L_d(k+1) \\ L_q(k+1) \end{bmatrix} = \begin{bmatrix} i_d(k) - \frac{T_sR_si_d(k)}{L_d(k)} + \frac{T_sp\omega_r(k)i_q(k)L_q(k)}{L_d(k)} + \frac{T_su_d(k)}{L_d(k)} \\ i_q(k) - \frac{T_s(-p)\omega_r(k)i_d(k)L_d(k)}{L_q(k)} - \frac{T_sR_si_q(k)}{L_q(k)} + \frac{T_su_q(k)}{L_q(k)} - \frac{T_s\psi_pp\omega_r(k)}{L_q(k)} \\ L_d(k) + T_s(\Theta_d(1)i_q(k)\tilde{i_d}(k) + \Theta_d(1)i_d(k)\tilde{i_q}(k) + \Theta_d(2)\tilde{i_d}(k) + \Theta_d(3)\tilde{i_q}(k)) \\ L_q(k) + T_s\big(\Theta_q(1)i_d(k)\tilde{i_q}(k) + \Theta_q(1)i_q(k)\tilde{i_d}(k) + \Theta_q(2)\tilde{i_d}(k) + \Theta_q(3)\tilde{i_q}(k)\big) \end{bmatrix}. \tag{26}$$

$$J_f(k+1) = \begin{bmatrix} \frac{\partial i_d(k+1)}{\partial i_d(k)} & \frac{\partial i_d(k+1)}{\partial i_q(k)} & \frac{\partial i_d(k+1)}{\partial L_d(k)} & \frac{\partial i_d(k+1)}{\partial L_q(k)} \\ \frac{\partial i_q(k+1)}{\partial i_d(k)} & \frac{\partial i_q(k+1)}{\partial i_q(k)} & \frac{\partial i_q(k+1)}{\partial L_d(k)} & \frac{\partial i_q(k+1)}{\partial L_q(k)} \\ \frac{\partial L_d(k+1)}{\partial i_d(k)} & \frac{\partial L_d(k+1)}{\partial i_q(k)} & \frac{\partial L_d(k+1)}{\partial L_d(k)} & \frac{\partial L_d(k+1)}{\partial L_q(k)} \\ \frac{\partial L_q(k+1)}{\partial i_d(k)} & \frac{\partial L_q(k+1)}{\partial i_q(k)} & \frac{\partial L_q(k+1)}{\partial L_d(k)} & \frac{\partial L_q(k+1)}{\partial L_q(k)} \end{bmatrix}. \tag{27}$$

$$J_f(k+1) = \begin{bmatrix} 1 - T_s\frac{R_s}{L_d(k)} & T_s\omega_{el}(k)\frac{L_q(k)}{L_d(k)} & J_{f_{13}} & T_s\omega_{el}(k)\frac{i_q(k)}{L_d(k)} \\ -T_s\omega_{el}(k)\frac{L_d(k)}{L_q(k)} & 1 - T_s\frac{R_s}{L_q(k)} & -T_s\omega_{el}(k)\frac{i_d(k)}{L_q(k)} & J_{f_{24}} \\ J_{f_{31}} & J_{f_{32}} & J_{f_{33}} & J_{f_{34}} \\ J_{f_{41}} & J_{f_{42}} & J_{f_{43}} & J_{f_{44}} \end{bmatrix}. \tag{28}$$

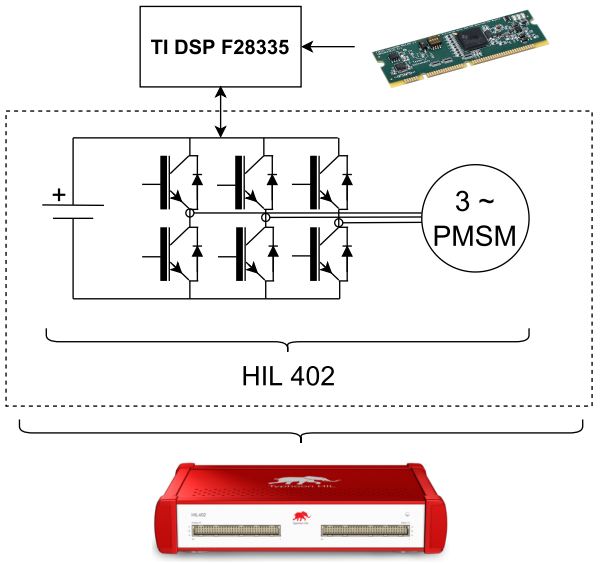

FIGURE 7. Experimental setup.

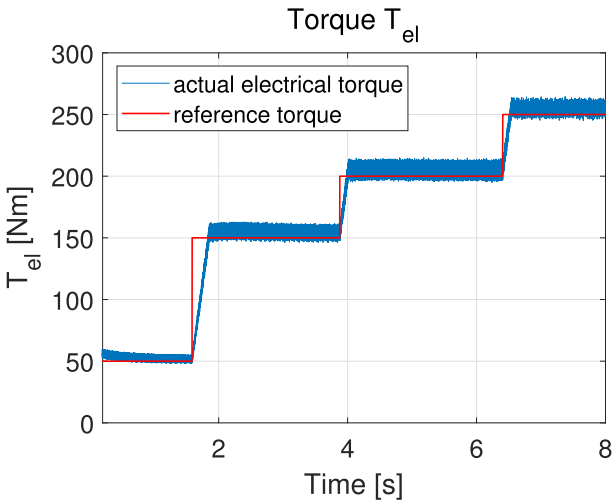

FIGURE 8. Actual machine electrical torque T_{el} for measurement with forward Euler discretisation.

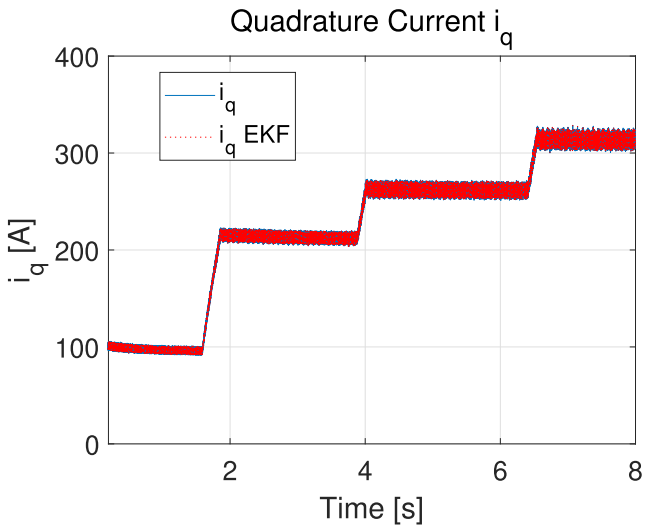

FIGURE 9. Estimated and actual values for forward Euler discretised quadrature current i_q.

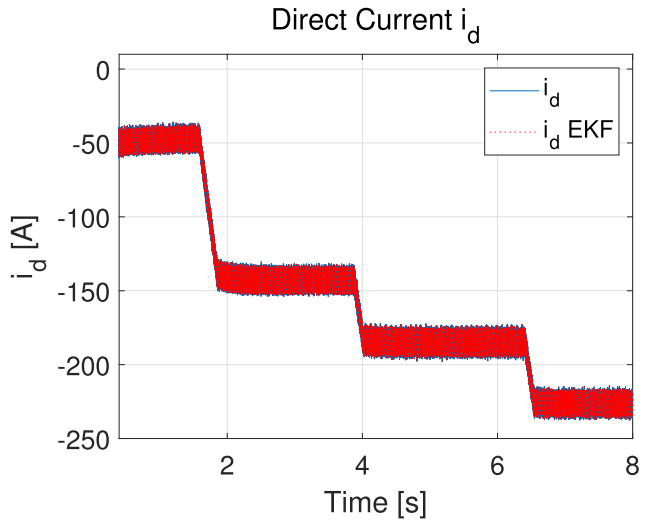

FIGURE 10. Estimated and actual values for forward Euler discretised direct current i_d.

For the currents i_d and i_q in Fig. 9 and in Fig. 10 the estimation process is without delay and very accurate due to the fact, that these values are measured in the input of the Kalman filter. The estimation process of L_q returns valid results right at the beginning of the control and becomes more accurate for a higher torque demand.

B. MEASUREMENT AND RESULTS WITH FORWARD EULER DISCRETISATION

The measurement results were taken for a desired torque between 50Nm and 250Nm in different steps. Fig. 8 displays the actual electrical machine torque T_{el} which is measured at the rotor of the PMSM. The torque ripple in Fig.8 is between 7% and 9%. The torque ripple is based on structural geometrical characteristics of the electrical machine. Contributions such as [32] as well as [33] indicate that a reduction of the torque ripple down to 9% becomes possible if some particular actions described, for instance, in these two papers are taken into account in the geometric design of the machine. As explained, the torque ripple is connected with structural geometric characteristics of the machine and cannot be reduced significantly below these values. The desired currents i_d and i_q are defined by an MTPA trajectory. The actual values for the estimated and measured current quantities are given in Fig. 9 and in Fig. 10. The current dependent nonlinear inductances are given in Fig. 11 and in Fig. 12, where the blue curve stands for the estimated inductance and the red curve for the actual inductance. The estimation process of L_d initially shows the same deviation as for L_q. Due to the small current values at low torque demands in the input of the EKF, the estimation process shows small deviations to

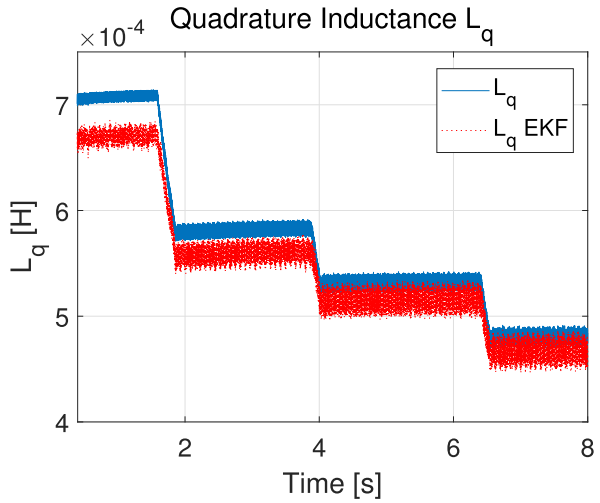

FIGURE 11. Estimated and actual values for forward Euler discretised quadrature inductance L_q.

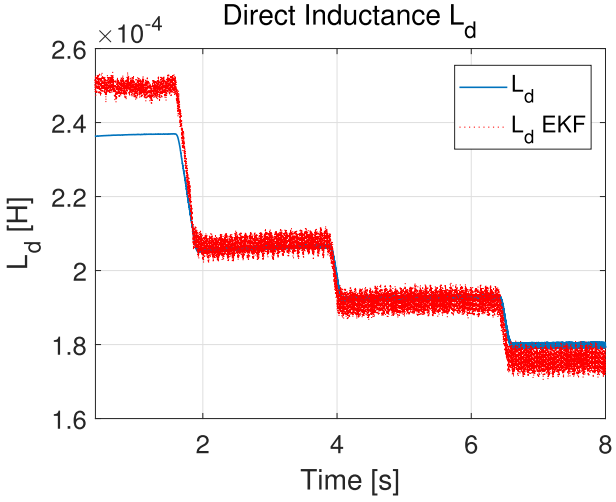

FIGURE 12. Estimated and actual values for forward Euler discretised direct inductance L_d.

the real existing values in the machine. Since the deviations are very small, they do not have a negative influence on the control.

VI. CONCLUSION

This paper deals with a combined extended Kalman filter by using a bivariate polynomial for the estimation of the saturated nonlinear states L_d and L_q in a permanent magnetic synchronous machine. The bivariate polynomial is calculated and considered in the estimation process using extended Kalman filters. A forward Euler discretisation is proposed in the extended Kalman filter's structure. Once L_d and L_q are estimated, continuous monitoring of saturation conditions of the machine through these estimations is conducted to guarantee the desired torque in saturation conditions. In fact, the proposed adaptive control scheme, based on MTPA with saturating optimal currents i_d and i_q as reference currents, consists of an adaptive feedforward and PI controller. Differences in between are discussed in light of measured results using Hardware-in-the-loop.

REFERENCES

[1] K. Asano, Y. Inaguma, H. Ohtani, E. Sato, M. Okamura, and S. Sasaki, "High performance motor drive technologies for hybrid vehicles," in *Proc. Power Convers. Conf. Nagoya*, Apr. 2007, pp. 1584–1589, doi: 10.1109/PCCON.2007.373175.

[2] *Two Million and Counting*, Global EV Outlook, International Energy Agency, Paris, France, 2017, p. 1.

[3] D. Schroeder, *Elektrische Antriebe-Regelung von Antriebssystemen*, vol. 4. Berlin, Germany: Springer, 2015, ch. 9, pp. 1095–1105.

[4] G. Pellegrino, E. Armando, and P. Guglielmi, "Direct-flux vector control of IPM motor drives in the maximum torque per voltage speed range," *IEEE Trans. Ind. Electron.*, vol. 59, no. 10, pp. 3780–3788, Oct. 2012, doi: 10.1109/TIE.2011.2178212.

[5] L. Sepulchre, M. Fadel, M. Pietrzak-David, and G. Porte, "MTPV flux-weakening strategy for PMSM high speed drive," *IEEE Trans. Ind. Appl.*, vol. 54, no. 6, pp. 6081–6089, Nov. 2018, doi: 10.1109/TIA.2018.2856841.

[6] T. Zwerger and P. Mercorelli, "Combining SMC and MTPA using an EKF to estimate parameters and states of an interior PMSM," in *Proc. 20th Int. Carpathian Control Conf. (ICCC)*, May 2019, pp. 1–6, doi: 10.1109/CarpathianCC.2019.8766063.

[7] T. Zwerger and P. Mercorelli, "Combining an internal SMC with an external MTPA control loop for an interior PMSM," in *Proc. 23rd Int. Conf. Methods Models Autom. Robot. (MMAR)*, Aug. 2018, pp. 674–679, doi: 10.1109/MMAR.2018.8485900.

[8] T. Zwerger and P. Mercorelli, "Combining a PI controller with an adaptive feedforward control in PMSM," in *Proc. 21st Int. Carpathian Control Conf. (ICCC)*, Oct. 2020, pp. 1–5, doi: 10.1109/ICCC49264.2020.9257288.

[9] T. Zwerger and P. Mercorelli, "A control scheme for PMSMs using model predictive control and a feedforward action in the presence of saturated inputs," in *Proc. 22nd Int. Carpathian Control Conf. (ICCC)*, May 2021, pp. 1–6, doi: 10.1109/ICCC51557.2021.9454662.

[10] R. Nalepa and T. Orlowska-Kowalska, "Optimum trajectory control of the current vector of a nonsalient-pole PMSM in the field-weakening region," *IEEE Trans. Ind. Electron.*, vol. 59, no. 7, pp. 2867–2876, Jul. 2012, doi: 10.1109/TIE.2011.2116755.

[11] J. Lee, K. Nam, S. Choi, and S. Kwon, "A lookup table based loss minimizing control for FCEV permanent magnet synchronous motors," in *Proc. IEEE Vehicle Power Propuls. Conf.*, Sep. 2007, pp. 175–179, doi: 10.1109/VPPC.2007.4544120.

[12] D.-Y. Kim and J.-H. Lee, "Low cost simple look-up table-based PMSM drive considering DC-link voltage variation," *Energies*, vol. 13, no. 15, p. 3904, Jul. 2020, doi: 10.3390/en13153904.

[13] Y. Yu, X. Huang, Z. Li, M. Wu, T. Shi, Y. Cao, G. Yang, and F. Niu, "Full parameter estimation for permanent magnet synchronous motors," *IEEE Trans. Ind. Electron.*, vol. 69, no. 5, pp. 4376–4386, May 2022, doi: 10.1109/TIE.2021.3078391.

[14] J. Zhang, F. Peng, Y. Huang, Y. Yao, and Z. Zhu, "Online inductance identification using PWM current ripple for position sensorless drive of high-speed surface-mounted permanent magnet synchronous machines," *IEEE Trans. Ind. Electron.*, vol. 69, no. 12, pp. 12426–12436, Dec. 2022, doi: 10.1109/TIE.2021.3130327.

[15] T. Boileau, N. Leboeuf, B. Nahid-Mobarakeh, and F. Meibody-Tabar, "Online identification of PMSM parameters: Parameter identifiability and estimator comparative study," *IEEE Trans. Ind. Appl.*, vol. 47, no. 4, pp. 1944–1957, Jul./Aug. 2011, doi: 10.1109/TIA.2011.2155010.

[16] G. Feng, C. Lai, and N. C. Kar, "A novel current injection-based online parameter estimation method for PMSMs considering magnetic saturation," *IEEE Trans. Magn.*, vol. 52, no. 7, pp. 1–4, Jul. 2016, doi: 10.1109/TMAG.2016.2525805.

[17] J. Lavenius and L. Vanfretti, "PMU-based estimation of synchronous machines' unknown inputs using a nonlinear extended recursive three-step smoother," *IEEE Access*, vol. 6, pp. 57123–57136, 2018, doi: 10.1109/ACCESS.2018.2873572.

[18] G. Welch and G. Bishop, "An introduction to the Kalman filter," Univ. North Carolina Chapel Hill, Chapel Hill, NC, USA, Tech. Rep. 95-041, 1995. [Online]. Available: http://www.cs.unc.edu/~welch/kalman/kalmanIntro.html

[19] M. Koteich, G. Duc, A. Maloum, and G. Sandou, "Observability of sensorless electric drives," 2016, *arXiv:1602.04468*.

[20] P. Vaclavek, P. Blaha, and I. Herman, "AC drive observability analysis," *IEEE Trans. Ind. Electron.*, vol. 60, no. 8, pp. 3047–3059, Aug. 2013, doi: 10.1109/TIE.2012.2203775.
[21] M. Koteich, A. Maloum, G. Duc, and G. Sandou, "Discussion on 'AC drive observability analysis,'" *IEEE Trans. Ind. Electron.*, vol. 62, no. 11, pp. 7224–7225, Nov. 2015, doi: 10.1109/TIE.2015.2438777.
[22] L. Mercorelli, "A hysteresis hybrid extended Kalman filter as an observer for sensorless valve control in camless internal combustion engines," *IEEE Trans. Ind. Appl.*, vol. 48, no. 6, pp. 1940–1949, Nov./Dec. 2012.
[23] P. Mercorelli, "A two-stage augmented extended Kalman filter as an observer for sensorless valve control in camless internal combustion engines," *IEEE Trans. Ind. Electron.*, vol. 59, no. 11, pp. 4236–4247, Nov. 2012.
[24] P. Mercorelli, "A motion-sensorless control for intake valves in combustion engines," *IEEE Trans. Ind. Electron.*, vol. 64, no. 4, pp. 3402–3412, Apr. 2017, doi: 10.1109/TIE.2016.2598314.
[25] P. Mercorelli, "A two-stage sliding-mode high-gain observer to reduce uncertainties and disturbances effects for sensorless control in automotive applications," *IEEE Trans. Ind. Electron.*, vol. 62, no. 9, pp. 5929–5940, Sep. 2015.
[26] B. Haus, P. Mercorelli, and H. Aschemann, "Gain adaptation in sliding mode control using model predictive control and disturbance compensation with application to actuators," *Information*, vol. 10, no. 5, p. 182, May 2019, doi: 10.3390/info10050182.
[27] M. Taherzadeh, M. A. Hamida, M. Ghanes, and M. Koteich, "A new torque observation technique for a PMSM considering unknown magnetic conditions," *IEEE Trans. Ind. Electron.*, vol. 68, no. 3, pp. 1961–1971, Mar. 2021, doi: 10.1109/TIE.2020.2972429.
[28] M. Bronstein, *Solving Polynomial Equations: Foundations, Algorithms, and Applications*. Trenton, NJ, USA: Springer, 2006.
[29] H. Liu, F. Hu, J. Su, X. Wei, and R. Qin, "Comparisons on Kalman-filter-based dynamic state estimation algorithms of power systems," *IEEE Access*, vol. 8, pp. 51035–51043, 2020, doi: 10.1109/ACCESS.2020.2979735.
[30] *TyphoonHIL 402 Hardware-in-the-Loop Device*. Accessed: Jan. 19, 2022. [Online]. Available: https://www.typhoon-hil.com
[31] C. Rommel, *HIL TESTED Powerful Performance, Functionality, and Quality From Model-Based Testing*. Somerville, MA, USA: Typhoon HIL, Jun. 2021. [Online]. Available: https://info.typhoon-hil.com/thank-you-white-paper-vdc-research-hil-tested?submissionGuid=2bbe68f7-6394-4511-9af9-fb437bb8595a
[32] K.-C. Kim, "A novel method for minimization of cogging torque and torque ripple for interior permanent magnet synchronous motor," *IEEE Trans. Magn.*, vol. 50, no. 2, pp. 793–796, Feb. 2014, doi: 10.1109/TMAG.2013.2285234.
[33] H. M. Kim, Y.-J. Kim, and S.-Y. Jung, "Torque ripple and back EMF harmonic reduction of IPMSM with asymmetrical stator design," in *Proc. 20th Int. Conf. Electr. Mach. Syst. (ICEMS)*, Aug. 2017, pp. 1–4, doi: 10.1109/ICEMS.2017.8056477.

TANJA ZWERGER received the Master of Engineering degree in electromobility and energy systems from the Ulm Professional School, in 2016. She is currently pursuing the Ph.D. degree with the University of Lueneburg, Germany. In 2016, she started as an Electrical Engineer at Rolls Royce Power Systems, Friedrichshafen, and was responsible for electrical system integration in the off-highway project for partial electrification in the train and marine sector. Since 2018, she has been a Senior Researcher at the Rolls Royce Research Center, Friedrichshafen, Germany. Her research interests include Kalman filters, sliding mode control, and model predictive control in applications for permanent magnet synchronous machines.

PAOLO MERCORELLI (Member, IEEE) received the Ph.D. degree in systems engineering from the University of Bologna, Bologna, Italy, in 1998. In 1997, he was a Visiting Researcher for one year with the Department of Mechanical and Environmental Engineering, University of California, Santa Barbara, CA, USA. From 1998 to 2001, he was a Postdoctoral Researcher with Asea Brown Boveri Corporate Research, Heidelberg, Germany. From 2002 to 2005, he was a Senior Researcher with the Institute of Automation and Informatics, Wernigerode, Germany, where he was the Leader of the Control Group. From 2005 to 2011, he was an Associate Professor in process informatics with the Ostfalia University of Applied Sciences, Wolfsburg, Germany. Since 2012, he has been the Distinguished Full Professor and the Chair of Control and Drive Systems with the Institute of Product and Process Innovation, Leuphana University of Lueneburg, Lueneburg, Germany. Since 2018, he has been an International Distinguished Visiting Professor with the Institute of Automatic Control, Lodz University of Technology, Lodz, Poland. His current research interests include applications of Kalman filters, robotics, wavelets, geometric control, and SMC. He was a recipient of a three year scholarship from the Marie Curie Actions Research Fellowship Program which is one of the most competitive and prestigious European awards sponsored by the European Commission, in 1998. He received seven best international conferences paper awards, such as IECON 2013, IECON 2014, CoDIT 2014, ICCC 2017, FedCSIS 2019, ACD 2019, and ICCC 2020. In the years 2019, 2020, 2021, and 2022, he has been on the list of the top 2% scientists by Elsevier Database. Since 2022, he has been the Editor-in-Chief for the Section *Journal of Engineering Mathematics* in *Journal of Mathematics*, an Open Access Journal from MDPI, Basel, and Switzerland.